In Vitro Nucleotide Misinsertion Opposite the Oxidized Guanosine Lesions Spiroiminodihydantoin and Guanidinohydantoin and DNA Synthesis Past the Lesions Using *Escherichia coli* DNA Polymerase I (Klenow Fragment)†

Olga Kornyushyna, Aym M. Berges, James G. Muller, and Cynthia J. Burrows*

Department of Chemistry, University of Utah, 315 South 1400 East, Salt Lake City, Utah 84112-0850

Received July 22, 2002; Revised Manuscript Received October 28, 2002

ABSTRACT: The low redox potential of 8-oxo-7,8-dihydroguanine (OG), a molecule regarded as a marker of oxidative damage in cells, makes it an easy target for further oxidation. Using a temperature-dependent method of synthesis, the oxidation products of OG, guanidinohydantoin (Gh) and/or its isomer iminoallantoin (Ia) as well as spiroiminodihydantoin (Sp), have been site-specifically incorporated into DNA oligomers. Single nucleotide insertion and primer extension experiments using *Escherichia coli* Kf exo$^-$ DNA polymerase were carried out under "standing start" and "running start" conditions in various sequence contexts. dAMP and dGMP were found to be inserted opposite these OG oxidation products. Steady-state kinetic studies show that the Gh/Ia·G base pair yields a lower K_m value compared to the Sp·G pair or X·A (X = Gh/Ia or Sp). Running start experiments using oxidized and unoxidized OG-containing templates showed enhanced full extension in the presence of all four dNTPs. A sequence preference for efficiency of extension was found when Gh/Ia and Sp are present in the DNA template, possibly leading to primer misalignment. Full extension is more efficient for the templates containing two Gs immediately 3′ to the lesions compared to two As. Although these lesions cause a significant block for DNA elongation, results show that they are more easily bypassed by the polymerase when situated in the appropriate sequence context. UV melting studies carried out on duplexes mimicking the template/primer systems were used to characterize thermal stability of the duplexes. These experiments suggest that both Gh/Ia and Sp destabilize the duplex to a much greater extent than OG, with Sp being most severe.

Endogenously generated oxygen radicals significantly contribute to the mutagenic process in cells by damaging DNA as well as the nucleotide triphosphate pool (*1*). Oxidative DNA damage results in strand breaks, abasic sites, DNA−protein cross-links, and oxidized bases, all of which require the action of DNA repair pathways to maintain the integrity of the genome. Under in vitro conditions, lesions present in the DNA template strand can severely impair DNA synthesis by blocking either one nucleotide before or across from the lesion site. In vivo, persistent DNA lesions often pose considerable obstacles to genome duplication, which can have lethal consequences for dividing cells (*2*). A large family of structurally related lesion-replicating polymerases that allow translesion DNA synthesis have been identified during the past decade, some of them highly error prone (*2*, *3*). Furthermore, intracellular oxidative damage of DNA is known to cause a significant increase in the overall polymerase error rate (*4*, *5*). Ultimately, the ability to continue replication in the presence of damage, and mistakes made by polymerases in the absence of DNA repair, can lead to mutagenesis.

Oxidative damage to DNA continues to receive a very high level of attention because of its relevance to cancer, aging, and neurological disorders (*6*, *7*). The mutational spectra associated with oxidative damage indicate that the most common base substitution is G·C → A·T transitions followed by G·C → T·A and G·C → C·G transversions, although the specific details of mutational frequencies depend on the reactive species (*8*). One molecular origin of G·C → T·A transversions is 8-oxo-7,8-dihydroguanine (OG),[1] a molecule widely regarded as the biomarker of oxidative damage in the cell (*9*, *10*). Depending upon the polymerase, either A or C may be inserted opposite OG during replication and transcription (*10*, *11*). The repair of the OG·A mismatch relies on the "GO" repair enzymes (*13*) that have been characterized in *Escherichia coli* (*15*). MutY protein from *E. coli* removes the unmodified adenine when it is paired with the OG, and another protein, MutT, is responsible for prevention of dOGTP incorporation into DNA. In double-stranded DNA, the OG·C base pair is repaired by the MutM protein, also known as Fpg, by removal of the OG lesion. Functional homologues to the *E. coli* MutM protein that show similar substrate specificities have been identified and characterized in yeast, yOgg1 and yOgg2 (*16*), and to some

† This work was supported by the NIH (CA90689). Funds from the NSF (CHE-9807669) and the University of Utah Institutional Funds Committee were provided for purchase of the mass spectrometer used in this study.

* Corresponding author. Phone: (801) 585-7290. Fax: (801) 581-8433. E-mail: burrows@chem.utah.edu.

[1] Abbreviations: OG, 8-oxo-7,8-dihydroguanine; Gh, guanidinohydantoin; Ia, iminoallantoin; Sp, spiroiminodihydantoin; Kf exo$^-$, *Escherichia coli* Klenow fragment of polymerase I lacking 3′→5′ exonuclease; Ab, abasic site; TLS, translesion synthesis.

10.1021/bi0264925 CCC: $22.00
Published on Web 11/28/2002

Scheme 1: Oxidation of OG to Gh/Ia and Sp

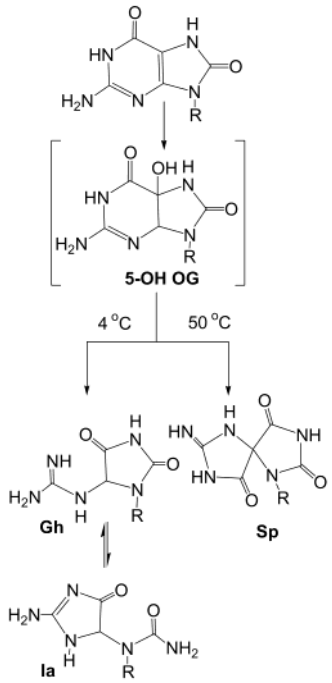

extent in mammalian cells, e.g., mOgg1 and hOgg1 (*14*, *18*). In recent years, many studies have been published aimed at establishing a correlation between the recognition of OG by the polymerases and repair enzymes and its impact on the conformation and thermodynamic stability of the DNA duplex (*19*−*22*). The influence of the base sequence flanking the damaged site on replication and repair is also a theme of intensive research (*2*, *4*, *23*−*25*).

Owing to its low redox potential, OG is highly susceptible toward further oxidation, and several in vitro studies now claim OG as a "hot spot" for oxidative damage (*5*, *26*, *27*). Thus, the subsequent chemistry of 8-oxo-7,8-dihydroguanosine oxidation and the potential mutagenicity of its oxidation products are of particular interest. Nucleoside studies in this laboratory have recently identified two major pathways of OG one-electron oxidation that lead to the formation of spiroiminodihydantoin (Sp) or to guanidinohydantoin (Gh) as shown in Scheme 1 (*28*). Importantly, these lesions also appear to arise from direct oxidation of deoxyguanosine by type I (*28*) and type II photooxidation (*30*) and peroxyl radicals (*32*) as well as through the action of a variety of other oxidants on OG (*30*, *33*−*35*). Indeed, Sp was mistakenly identified as 4-hydroxy-8-oxo-7,8-dihydroguanosine for more than a decade (*9*, *31*, *32*, *36*, *37*). The formation of Gh is further complicated by its possible isomerization to iminoallantoin (Ia), and the structure is hereafter referred to a Gh/Ia (*29*). The predominant isomer in duplex DNA has yet to be determined and may be dependent upon base pairing and sequence context.

Further studies of short oligodeoxynucletides have shown that oxidation of OG in duplex DNA led to the formation of Gh/Ia as the major products. In single-stranded oligodeoxynucleotides, the reaction was highly temperature dependent, leading to Gh/Ia at low temperature and Sp at high temperature (*29*, *38*). Our first qualitative assessment of the potential for miscoding of the new lesions showed insertion of dAMP > dGMP ≫ dCMT, dTMP opposite a mixture of oxidized

a) Template 1/Primer 5: X= G, OG, Gh/Ia, Sp, or Ab site

```
5′-dTCATGGGTCXTCGGTATATCAGTGCTATCACATTAGTGTA-3′
              AGCCATATAGTCACGATAGT-5′
```

Template 2/Primer 6: X= OG, Gh/Ia, or Sp

```
5′-dTCATGGGTCXAAGGTATATCAGTGCTATCACATTAGTGTA-3′
               CCATATAGTCACGATAGTGT-5′
```

Template 3/Primer 7: X= OG, Gh/Ia, or Sp

```
5′-dTCATGGGTCXGGCGTATATCAGTGCTATCACATTAGTGTA-3′
               GCATATAGTCACGATAGTGT-5′
```

Template 3/Primer 8: X= OG, Gh/Ia, or Sp

```
5′-dTCATGGGTCXGGCGTATATCAGTGCTATCACATTAGTGTA
                         TCACGATAGTGTAATCACAT-5′
```

b) G-C rich sequences:

```
5′-GAC CXG GTC AGT GCT ACT-3′ <-XGG18
     | ||| ||| ||| ||| |||
       C CAG TCA CGA TGA-5′ <-CC13
      NC CAG TCA CGA TGA-5′ <-CC14N
    G GNC CAG TCA CGA TGA-5′ <-CC16N
                             (N=A, C, G, T)
X = G, OG, Sp, or Gh/Ia
```

A-T rich Sequences:

```
5′-GAT TXA ATC AGT GCT ACT-3′; <-XAA18
    | ||| ||| ||| ||| |||
      T TAG TCA CGA TGA-5′ <-TT13
     NT TAG TCA CGA TGA-5′ <-TT14N
  A ANT TAG TCA CGA TGA-5′ <-TT16N
                           (N=A, C, G, T)
X = G, OG, Sp, or Gh/Ia
```

FIGURE 1: Sequences of templates and primers employed in these studies.

products (*39*). The temperature-dependent method for synthesis of pure Sp vs Gh/Ia-containing oligos allowed us now to carry out a more careful analysis of these lesions independently and in a variety of sequence contexts.

In the present work, we used the Klenow fragment of DNA polymerase I deficient in exonuclease activity (Kf exo$^-$) to study single nucleotide insertion and primer extension at the oxidized lesions in different sequence contexts (Figure 1a). The results of the "running start" primer extension experiments (in which DNA synthesis proceeds normally for a few base pairs before a lesion is encountered) suggest a correlation between the sequence context surrounding the lesion and the efficiency of its bypass by the polymerase. To further investigate this idea, we performed UV melting experiments to characterize the stability of numerous DNA duplexes containing either guanine, OG, Gh/Ia, or Sp in various sequence contexts (Figure 1b). Two 18-mer templates were annealed to primers of various lengths (13-mers, 14-mers, and 16-mers) to compare how increased hydrogen-bonding and base-stacking interactions around the lesion site affected duplex stability.

EXPERIMENTAL PROCEDURES

Materials and Instrumentation. Reagents and enzymes were purchased from the following sources: Na_2IrCl_6 from Alfa Aesar (Ward Hill, MA), dOG and dU phosphoramidites

from Glen Research (Sterling, VA), dNTPs from Pharmacia (Piscataway, NJ), and [γ-^{32}P]ATP from Amersham (Arlington Heights, IL). T4 polynucleotide kinase, Klenow fragment (3′→5′ exo$^-$), DNA pol I, and uracil−DNA glycosylase (UDG) were from New England Biolabs (Beverly, MA). ESI mass spectra were recorded on a Micromass Quattro II. UV thermal denaturing studies were monitored on a Beckman DU7400 UV−vis spectrophotometer. Phosphorimagery was performed on a Molecular Dynamics Model 860.

Oligodeoxynucleotide Synthesis. Deoxyribonucleotides with or without modification were synthesized using standard automated solid-support chemistry protocols on an Applied Biosystems Model 392B synthesizer using the manufacturer's protocols. Oligomers containing OG were deprotected in concentrated NH_4OH with 0.25 M β-mercaptoethanol (in order to prevent undesired oxidation of OG) at 65 °C for 17 h, after which NH_3 was removed in vacuo. Gel electrophoresis on 15% or 20% polyacrylamide gels with 7 M urea provided the purified oligonucleotides. The purity of synthesized and modified duplexes was confirmed by ESI mass spectral analysis. A 40-mer containing a single abasic site was prepared using uracil−DNA glycosylase (UDG) as follows: 6 μg of a uracil-containing 40-mer was incubated for 2 h at 37 °C with 10 units of UDG in the reaction mixture containing 70 mM HEPES, 50 mM EDTA, and 1 mM dithiothreitol (pH 7.4) (*40*). Hot treatment (90 °C) with 0.1 M piperidine for 60 min and subsequent gel electrophoresis analysis confirmed that 100% of deoxyuracil was converted to an abasic site yielding alkali-induced strand scission. The uracil-containing oligonucleotide was sequenced by 75 μM $KMnO_4$ (T-sequencing reaction) and dimethyl sulfate (A + G sequencing reactions) prior to UDG treatment.

DNA Oxidation with Na_2IrCl_6. Mass Spectrometric Analysis of the Oxidation Products. Selective oxidation yielding either Sp or Gh/Ia was achieved by treating 500 μL samples containing the corresponding OG-containing oligodeoxynucleotides (12 μM) (Figure 1) with 2 μL of 25 μM Na_2IrCl_6, giving a final concentration of 100 μM Na_2IrCl_6. Specifically, Sp was generated at 65 °C in a 10 mM sodium phosphate (NaP_i)/100 mM NaCl buffer at pH 7.0, whereas an equilibrating mixture of Gh + Ia was generated at 4 °C in a 10 mM NaP_i/100 mM NaCl buffer at pH 6.0. These reactions were incubated at their corresponding temperatures for 30 min when they were quenched by addition of a 4 μM amount of 20 mM EDTA (pH = 8.5). The reactions were pooled and dialyzed (2 kDa MWCO) against water for 24−48 h. The recovered solution was lyophilized to dryness and resuspended in 50 μL of water and 50 μL of 10 M NH_4OAc. After 2 h at room temperature, 300 μL of a cold mixture of 2-propanol and ethanol (1:1) was added, and the DNA was incubated for at least 8 h at −80 °C. The sample then was centrifuged for 30 min at 4 °C, and the supernatant liquid was carefully removed, leaving the DNA as a pellet. This pellet was lyophilized to dryness and dissolved in 50 μL of 1 mM ammonium acetate and 100 μL of 2-propanol. This sample was used for mass spectral analysis; additionally, a portion of this sample before NH_4OAc exchange was 5′-radiolabeled with ^{32}P, subjected to hot piperidine treatment (1 M, 60 min), and analyzed by gel electrophoresis to establish strand integrity. HPLC analysis indicated that <1% OG remained in the Ir(IV)-oxidized oligomers, although no OG was detectable by mass spectrometry. Template **1** with X = Gh/Ia was 98% pure with small impurities of OG and Sp, as analyzed by HPLC (see Supporting Information). Template **1** with X = Sp was 90% pure with the principal impurity being Gh/Ia (see Supporting Information). These samples were used for the majority of kinetic studies described herein. Further purification (see Supporting Information) did not change the kinetic interpretation.

End Labeling of Primers and Template/Primer Annealing. The 20-mer primers were 5′-end-labeled using T4 polynucleotide kinase and [γ-^{32}P]ATP. Unreacted [γ-^{32}P]ATP was separated from labeled oligonucleotides with MicroSpin G-25 columns (Amersham Pharmacia Biotech). The primers were annealed to the templates in 10 μL solutions of 1× EcoPol buffer (10 mM Tris-HCl, 5 mM $MgCl_2$, and 7.5 mM DTT, pH 7.5) with a template:primer nanomolar ratio of 6:1 for qualitative analysis and 3:1 for steady-state kinetic analysis, yielding a final concentration of 225 and 75 nM for template and primer, respectively.

Single Nucleotide Insertion and Primer Extension. "Standing start" single nucleotide insertion and primer extension reactions (as illustrated in Figure 1, template **1**/primer **5**) were catalyzed by DNA polymerase Klenow fragment (Kf exo$^+$) and Klenow fragment (3′→5′ exo$^-$). DNA polymerization reactions were initiated by mixing a solution containing the template/primer mixture, a solution of DNA polymerase, and a mixture of all four dNTPs or a single dNTP. The final concentrations were 15 nM for template/primer, 0.2 unit (12.5 nM) for the enzyme, and 30 μM for a single dNTP or a mixture of all four dNTPs. Reaction mixtures were incubated at 37 °C for 15 min.

All running start DNA polymerization reactions (Figure 1, template **2**/primer **6**, template **3**/primer **7**, and template **3**/primer **8**) were catalyzed by Kf exo$^-$. In this set of experiments a 30 M mixture of a single dNTP plus dTTP (or dCTP) for insertion opposite the two As (or Gs) upstream to the lesion or a mixture of all for dNTPs was used. Reactions were also incubated with 0.2 unit of Kf exo$^-$ at 37 °C for 15 min.

All reactions were quenched with 5.5 μL of termination solution (95% formamide, 0.1% bromophenol blue, and 0.1% xylene cyanol). The samples were heated at 90 °C for 3 min, applied onto a 15% polyacrylamide gel in the presence of 7 M urea, and then analyzed by phosphorimagery.

Steady-State Kinetics. Reactions run under steady-state conditions were all catalyzed by Kf exo$^-$. The conditions used were the same as for qualitative insertion studies. The annealed template/primer (**1/5**) was mixed with the diluted enzyme in the molar ratios of 4:1 for Gh/Ia and Sp-containing templates, 64:1 for the OG-containing template, and 200:1 for the unmodified template. The steady-state reactions with Kf exo$^-$ utilized 0.22 nM (∼0.0036 unit) enzyme for dCTP insertion opposite an unmodified G (**1/5**). Insertion of dCTP and dATP opposite OG (**1/5**) required 0.7 nM (∼0.01 unit) enzyme, while dGTP insertion opposite OG utilized 1.25 nM (∼0.02 unit) Kf exo$^-$. dATP and dGTP insertion into the template (**1/6**) oxidized at 4 and 65 °C required 12.5 nM (0.2 unit) enzyme. Amounts of polymerase used (0.0018−0.1 unit/μL) and reaction times (3−15 min) were adjusted to ensure "single-hit" conditions as described by Goodman et al. (*41*). dNTP concentrations were chosen to allow the Michaelis−Menten curves to reach a plateau. The reactions were quenched with 5.5 μL of a termination solution and

applied on the 15% denaturing polyacrylamide gel. Radiolabeled primer extension was quantified by phosphorimaging (Molecular Dynamics Storm 860). Relative velocities were calculated as described by Morales et al. (*42*). k_{cat} and K_m values were obtained by nonlinear regression fitting of the data points using KaleidaGraph version 3.09 (Synergy Software, Reading, PA). All of the experiments were performed at least three times.

UV Spectroscopy and Thermal Denaturation Studies. Samples (325 μL) for thermal denaturation studies contained a 1:1 molar ratio of template:primer, with a final duplex concentration of 5 μM. These solutions were prepared by adding stock solutions (32.5 μL of 50 μM) of the two complementary oligomers to 65 μL of 5× Tm buffer (50 mM NaPIPES, pH 7.0, 50 mM NaH_2PO_4, 500 mM NaCl), and 295 L of distilled H_2O, with a final volume of 325 μL. The complementary oligomers were then annealed by heating in a water bath to 90 °C for 5 min, followed by slow cooling over 3−4 h to room temperature; the solutions were then stored at 4 °C until used. The UV spectra and absorbance measurements were recorded on a Beckman DU7400 UV−vis spectrophotometer equipped with a 6 × 325 μL cuvette Peltier temperature controller (P/N 517447). Absorbances were monitored at 260 nm while the temperature was varied; specifically, following a 10 min incubation period at 10 °C the temperature was ramped (1 °C per min) up to 80 °C and back down to 10 °C over a 140 min period. The collected data were then converted to the fraction of duplexed DNA (*f*), through the equation: $f = (A - A_{SS})/(A_{DS} - A_{SS})$, where *A* is the absorbance of sample at a particular temperature, A_{SS} is the average single-stranded absorbance, and A_{DS} is the average double-stranded absorbance. These data were used to generate a plot of *f* versus temperature graphed near the T_m temperature where $f = 50\%$. Subsequent linear regression determined the T_m from the equation of the line where the fraction of DNA duplexed is 0.5. Using these data, equilibrium constants at each data point were calculated as follows (*43*): $K = f/(2(1 - f)^2)C_T$, where *f* is the fraction of DNA duplexed for that particular temperature and C_T is the strand concentration for a single strand (5 μM). Linear regression analysis of a graph of ln *K* versus 1/*T* plotted near the T_m values yielded the equilibrium constants (*K*). The Gibbs free energy, ΔG^{37}, was then calculated by using the relationship: $\Delta G^{37} = -RT \ln K$, where $R = -1.987$ kcal/(mol·K), and $T = 310$ K. All denaturing experiments were repeated a minimum of three times in order to achieve an acceptable standard deviation. To compare how the addition of either one or two bases affected thermal stability, ΔT_m values were calculated as follows: $\Delta T_m = T_{m(14-mer\ or\ 16-mer)} - T_{m(13-mer)}$

RESULTS

Qualitative Analysis of Standing Start Single Nucleotide Insertion and Primer Extension Opposite Oxidized OG. Template **1** and its $IrCl_6^{2-}$ oxidized products obtained at 4 and 65 °C were purified and subjected to ESI-MS analysis (Figure 2). The largest peak in the spectrum obtained from low-temperature oxidation represents a loss of 10 Da from the mass of the starting material (12337.3 Da). This product was assigned to be guanidinohydantoin, Gh, and/or its equilibrium isomer iminoallantoin, Ia (*29*). The largest peak in the spectrum of the oligodeoxynucleotide **1** oxidized at

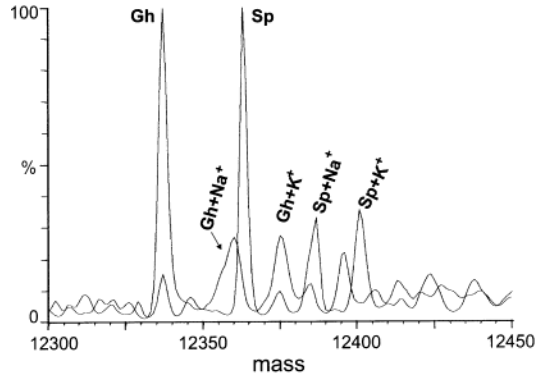

FIGURE 2: ESI-MS analysis of template **1** (X = OG) oxidized by Na_2IrCl_6 at 4 and 65 °C (see Experimental Procedures), yielding oligonucleotides containing Gh and Sp, respectively.

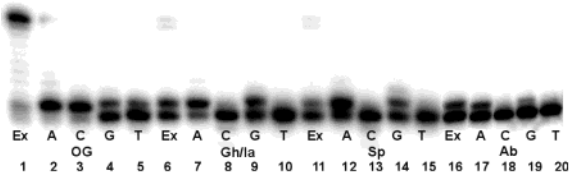

FIGURE 3: Nucleotide insertion opposite OG (lanes 1−5), Gh/Ia (lanes 6−10), and Sp (lanes 11−15) (duplex **1/6**) and an abasic site (lanes 16−20) (duplex **2/6**). Primer extension reactions were catalyzed by Kf exo$^-$ using a mixture of all dNTPs (lane Ex) or a single dNTP (lanes A, C, G, and T). Reactions conditions are described in the text.

65 °C occurred at a mass of 12363.3, representing an increase of 16 Da compared to the OG-containing starting material. On the basis of previous studies with nucleosides and short DNA oligomers this product was assigned as spiroiminodihydantoin, Sp (*28*). Although a trace of the starting material (OG) remained in template **1** with X = Gh/Ia after treatment with 100 M $IrCl_6^{2-}$ for 30 min, the Sp-containing oligomer was essentially free of OG. On the basis of the instrument sensitivity, the Gh/Ia- and Sp-containing DNA oligonucleotides were considered to be 98% and 90% pure, respectively. Small quantities of more highly purified materials (>98%) were also prepared for comparison (see Supporting Information).

To study insertion of dNTPs opposite oxidized forms of 8-oxo-7,8-dihydroguanosine in the 40-mer template (**1**), the oxidized template was annealed to a 20-mer primer (**5**) (Figure 1a). Primer extension was catalyzed by Kf exo$^-$ polymerase (0.2 unit) for 15 min at 37 °C in the presence of a mixture of all four dNTPs or a single dNTP. Template (**1**) with X = OG or Ab (abasic site) at position 10 from the 5′ end was used in control experiments for nucleotide insertion and primer extension. The same enzyme concentration and reaction conditions were used in each case.

The results of these experiments are shown in Figure 3. In the case of an unoxidized template (**1**, X = OG), the expected insertion of dAMP and dCMP opposite OG at position 10 was observed (lanes 2 and 3) (*11*). Under the reaction conditions used, approximately equal amounts of dAMP and dCMP were inserted. In the presence of all four dNTPs, the full-length product was obtained (lane 1); however, a small amount of polymerase dissociation from the OG site was also observed, resulting in a corresponding band on the gel.

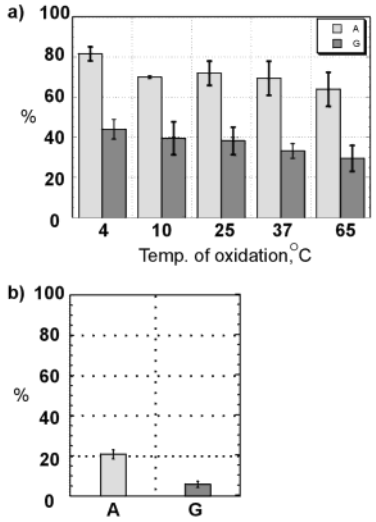

FIGURE 4: Temperature-dependent studies of the dAMP and dGMP insertion opposite oxidized OG (a) and the Ab site (b). OG containing template **1** was treated with Ir(IV) at different temperatures as described in the text, yielding Gh/Ia at 4 °C and Sp at 65 °C. Primer extension reactions were catalyzed by 0.2 unit of Kf exo$^-$ at 37 °C.

OG-containing template **1** could be selectively oxidized by $IrCl_6^{2-}$ at 4 and 65 °C, and the insertion of dAMP and dGMP was detected (Figure 3, lanes 7, 9, 12, and 14) as reported in previous studies (*39*). In the presence of all four dNTPs, oxidized forms of OG represented a strong block for primer extension, and only trace amounts of the full-length products were observed (Figure 3, lanes 6 and 11). Template **1** oxidized at 10, 25, and 37 °C provided similar results (data not shown). Interestingly, for higher temperatures of oxidation yielding predominantly Sp, the total amounts of dAMP and dGMP inserted decreased slightly (Figure 4).

To compare insertion of dAMP and dGMP opposite the products of OG oxidation to an abasic site, the template 40-mer (**1**) containing an abasic site at position "X" (Figure 1a) was designed. When template **1** was used under similar reaction conditions, we observed a preferential insertion of dAMP opposite the Ab site (Figure 3, lane 17). Under the conditions employed, insertion of dGMP was also detected but to a much smaller extent (Figure 3, lane 19). However, the relative amounts of dAMP and dGMP inserted opposite the Ab vs oxidized OG in our system were substantially different (Figure 4). When all four dNTPs were present, DNA synthesis was more strongly blocked by the Ab site (Figure 3, lane 16) compared to oxidized OG lesions.

To gain insight into the effect of lesion-containing DNA on the complete Klenow fragment retaining exonuclease activity, proofreading reactions were catalyzed by 0.2 unit of Kf exo$^+$ using primer **5** annealed to an unoxidized OG-containing template **1**, or with template **1** oxidized with Ir(IV) at 4 and 65 °C. Reactions were performed in the presence of a mixture of all four dNTPs or a single dNTP, and reaction conditions were the same as for the Kf exo$^-$ catalyzed reactions. Template **1** containing an unmodified G at position 10 annealed to primer **5** was used as a control in this experiment. Single nucleotide insertion and primer extension reactions with the **1/5** template/primer mixture catalyzed by Kf exo$^-$ were performed to compare the action of the two enzymes on a template with an unmodified G. Results of these experiments are shown in Figure 5. Both enzymes insert the correct dCMP opposite an unmodified G (lanes 3 and 8). Detectable background amounts of dTMP and dGMP were inserted opposite an unmodified G by Kf exo$^+$ (lanes 9 and 10). Bands corresponding to the degradation of the extended primer were also observed in this case. When a lower enzyme concentration (0.01 unit) was used, only the correct dCMP was inserted opposite G in the template (data not shown). Kf exo$^+$ inserted dAMP and dCMP opposite OG (lanes 12 and 13) as expected (*11*). In the presence of all four dNTPs (lane 11) the formation of the fully extended primer was detected. For template **1** (X = Gh/Ia, Sp), only background amounts of dAMP and dGMP insertion were observable opposite the lesions (lanes 17, 19, 22, and 24) and only trace amounts of the extended products were discovered in the presence of all four dNTPs (lanes 16 and 21). For reactions catalyzed by Kf exo$^+$, degradation of the extended primer was observed in lanes 9−25 in the presence of various dNTPs.

*Running Start Single Nucleotide Insertion and Primer Extension Opposite an Oxidized OG (Template **2**/Primer **6**).* It was anticipated that a polymerase given a running start in which normal DNA synthesis could proceed before encountering a lesion would lead to higher amounts of lesion bypass. To study single nucleotide insertion and primer extension under running start conditions, 40-mer templates **2** (Figure 1a), containing two As on the 3′ side of an OG, and **3**, with two Gs on the 3′ side of an OG, were selectively oxidized by $IrCl_6^{2-}$ at 4 and 65 °C. The 20-mer primers **6** and **7** were then annealed to the corresponding templates as shown in Figure 1a, allowing a running start for primer extension. DNA synthesis was catalyzed by 0.2 unit of Kf exo$^-$ at 37 °C for 15 min in the presence of a mixture of a single dNTP plus dTTP (or dCTP) or alternatively all four dNTPs for full

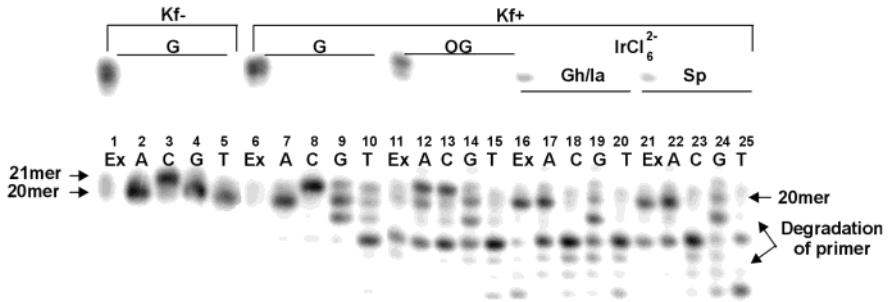

FIGURE 5: Single nucleotide insertion and primer extension reactions catalyzed by Kf exo$^-$ (lanes 1−5) and proofreading reactions catalyzed by Kf exo$^+$ (lanes 6−25). Duplex **3/6** was used as a substrate in lanes 1−10. Duplex **1/6** was used for proofreading studies opposite OG and its oxidized forms in lanes 11−25. All reactions were carried out as described in the text.

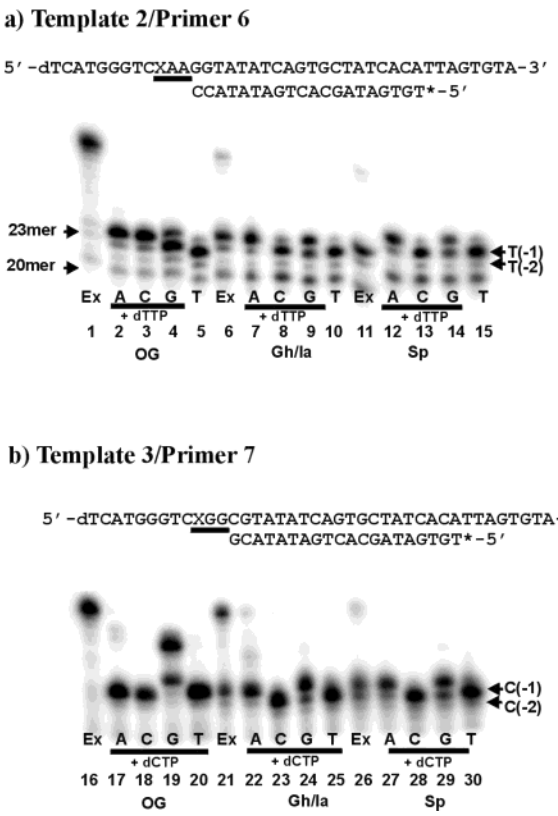

FIGURE 6: Running start DNA synthesis on **4/7** and **5/8** duplexes containing OG, Gh/Ia, or Sp. Reactions were catalyzed by 0.2 unit of Kf exo$^-$ as described in the text. X = OG (lanes 1−6 and 16−20), Gh/Ia (lanes 6−10 and 21−25), and Sp (lanes 11−15 and 26−30).

extension. Unoxidized templates, **2** and **3** (X = OG), were used for comparison.

Results of the running start DNA synthesis experiments are shown in Figure 6. In the case of an unoxidized template **2** containing OG, preferential insertions of dAMP and dCMP were observed, and a 20-mer primer **6** was extended to a 23-mer (Figure 6, lanes 2 and 3). We also detected a small amount of dGMP insertion opposite an unoxidized OG during DNA synthesis under the running start conditions (lane 4). In the presence of dTTP (lane 5), primer **6** was extended to a 22-mer. This result suggests that an unmodified OG downstream to the A does not influence insertion of the correct dTMP. In the presence of all four dNTPs the full-length product was obtained (lane 1). In the case of template **2** (Figure 6a) oxidized at 4 and 65 °C (X = Gh/Ia and Sp), dAMP and dGMP were preferentially inserted by Kf exo$^-$ (lanes 7, 9, 12, and 14). The correct dTMP was inserted opposite the two As upstream to the oxidized lesions (lanes 10 and 15). When all four dNTPs are present, full extension was efficiently blocked; however, detectable amounts of extended primer were obtained (lanes 6 and 11). In the case of the Gh/Ia- and Sp-containing template/primer systems, the extension products obtained migrated faster than those of the OG-containing system (lane 1 vs lanes 6 and 11).

Template/Primer Misalignment Is Observed for the Running Start Reactions with Template 3/Primer 7. The insertion pattern for template **3**/primer **7** differs from the template **2**/primer **6** system. For the unoxidized OG-containing template **3**/primer **7** and a mixture all four dNTPs, a fully extended primer was obtained with Kf exo$^-$ (Figure 6b, lane 16). As for template **2,** the insertion of dCMP was observed opposite OG in lane 18, corresponding to the formation of a 23-mer extended primer. The insertion of dCMP was also observed in lane 20 when a mixture of dTTP and dCTP was present. An intense band corresponding to the insertion of dAMP opposite the lesion (23-mer) was observed in lane 17 when a mixture of dATP and dCTP was added to the system. However, a low-intensity band with a slower mobility corresponding to a 28-mer was also detected in this lane. Even though the reaction mixture does not contain the substrate complementary to the C on the 5′ side of the lesion, the insertion of dAMP and dCMP complementary to the next five template bases apparently stabilizes misalignment of the extended primer. When a mixture of dGTP and dCTP was present, insertion of dCMP opposite the lesion was immediately followed by the subsequent insertion of the next correct dGMP opposite a C downstream to the lesion, and the resulting band corresponding to a 24-mer was observed (lane 19). The next template base (T) does not have a base-pairing partner in the reaction mixture, yet the synthesis did not stop at this point, and the polymerase proceeded to extend the primer to a 27-mer. It appears that misalignment insertion of the dCMPs opposite the triple G on the 5′ side facilitates further synthesis, probably causing the template T to loop out.

In the case of template **3** containing Gh/Ia, the band corresponding to the fully extended primer (Figure 6b, lane 21) displayed a noticeably higher intensity than that in lane 6. The insertion of dAMP was observed (lane 21). Interestingly, detectable amounts of the products extended past the lesion site were also present in lane 21. Primer misalignment might also have occurred in this case, since Gh/Ia is able to interact favorably with A to some extent, as evident from our insertion studies. dGMP was inserted opposite the Gh/Ia lesion as observed in lane 24. Again, a low-intensity band with a higher electrophoretic mobility was detected in this lane, suggesting that a misalignment insertion possibly takes place but to a smaller extent compared to lanes 19 and 21.

For template **3** oxidized at 65 °C (X = Sp) in the presence of all four dNTPs, the polymerase dissociates from the lesion site, causing a corresponding band on the gel; however, a detectable amount of the fully extended primer was observed in this case (lane 26). dAMP and dGMP were inserted opposite Sp in lanes 27 and 30, and background amounts of further extended primers were also present in these lanes.

Comparison of the Relative Amounts of Fully Extended Primers in Different Sequence Contexts. Since the running start experiments described above show that the amount of fully extended primer is a function of the upstream sequence context, additional primer extension reactions were performed. In addition to template/primer systems **1/5**, **2/6**, and **3/7** described above, primer **8** was annealed to template **3** at position 21 from the 5′ end (Figure 1a). Primer extension reactions catalyzed by Kf exo$^-$ in the presence of a 30 μM mixture of all four dNTPs were performed in triplicate for these various template/primer systems. The relative intensities of the bands corresponding to the fully extended primers were quantified by phosphorimagery (Figure 7). For unoxidized OG, full extension was the least efficient for the standing start **1/5** template/primer. The relative amounts of fully extended primers for unoxidized **2/6**, **3/7**, and **3/8** coincided within standard deviation. In the case of Gh/Ia and Sp, full

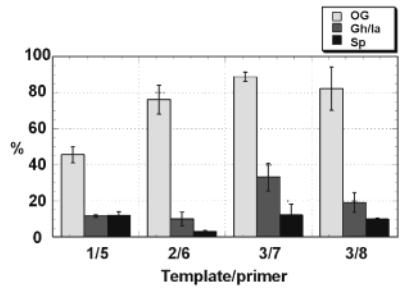

FIGURE 7: Comparison of the relative amounts of fully extended primers. Reactions were catalyzed by 0.2 unit of Kf exo$^-$ and were carried out in the presence of all four dNTPs (see Experimental Procedures).

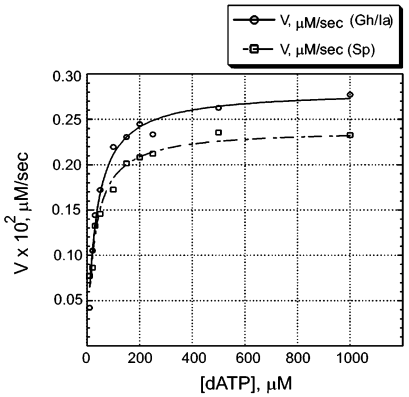

FIGURE 8: Representative plot of the reaction velocities for the single nucleotide insertion. dNTP concentrations were chosen to allow the Michaelis−Menten curves to reach a plateau (see Experimental Procedures). The plot is shown for dATP insertion opposite Gh/Ia and Sp.

extension appears to be most efficient for the templates containing two Gs immediately 3′ to the oxidized lesion. To ensure that full extension for the oxidized systems was not due to the presence of a trace amount of unreacted OG, single nucleotide insertion of dCMP was used as a control. dCMP insertion was never observed for the oxidized lesions (Figures 1a and 6; the results for the **3/8** template/primer system are not shown). In addition, full extension was reanalyzed using HPLC-purified template **1** (X = Gh/Ia or the individual diastereomers of Sp), and the data were essentially the same (see Supporting Information).

Steady-State Kinetics of dNMP Insertion Opposite G, OG, Gh/Ia, and Sp. Steady-state assays with Kf exo$^-$ were carried out in order to quantitate the differences observed in single nucleotide insertion opposite an unmodified G, OG, Gh/Ia, and Sp.[2] Reaction velocities (Figure 8) were determined at various substrate concentrations (see Experimental Procedures), and the values of k_{cat}, the kinetic rate constant for the ensemble of processes of enzyme-bound species, and K_m were determined for each lesion (Table 1). The relative

[2] Small samples of HPLC-purified template **1** containing either Gh/Ia or Sp could also be obtained. In the case of Sp, the two diastereomers arising from the quaternary carbon of the heterocycle could also be separated to >98% purity. When the steady-state kinetic experiments were repeated for dATP insertion using these templates, the data for Gh/Ia and Sp1 (the faster eluting diastereomer) were within experimental error of the values presented in Table 1, while k_{cat}/K_m for Sp2 (the slower eluting diastereomer) was diminished by a factor of only 3 (see Supporting Information). We conclude that the purity of the lesion-containing oligomers originally obtained is sufficient to draw the conclusions presented herein.

Table 1: Steady-State Kinetic Parameters of dNTP Insertion Opposite the Lesions

	K_m (μM)	k_{cat} (s^{-1})	k_{cat}/K_m (s^{-1} μM^{-1})	f
G·C	0.2 ± 0.02	0.14 ± 0.004	0.70	
OG·C	0.3 ± 0.05	0.011 ± 0.0001	0.04	
OG·A	0.63 ± 0.03	0.012 ± 0.0002	0.019	0.47
OG·G	48 ± 12	0.009 ± 0.0006	18×10^{-5}	0.003
Gh·A	34 ± 3.6	0.0028 ± 0.0001	8.2×10^{-5}	—[a]
Gh·G	2.9 ± 0.9	0.0023 ± 0.0001	79×10^{-5}	—[a]
Sp·A	29 ± 3.4	0.0024 ± 0.0001	8.3×10^{-5}	—[a]
Sp·G	16 ± 1.9	0.0018 ± 0.0003	10×10^{-5}	—[a]

[a] There was <1% dCTP insertion observed opposite Gh and Sp ($k_{cat}/K_m < 10^{-7}$).

catalytic efficiencies (k_{cat}/K_m) of dCTP insertion opposite an unmodified G (duplex **1/5**) and OG were 18-fold different. The insertion of dCTP opposite an unoxidized OG (duplex **1/5**) was twice as efficient as that of dATP and >200-fold more efficient than dGTP insertion. The misinsertion frequencies (f) of Kf exo$^-$ were determined to be 0.47 for dATP and 0.003 for dGTP insertion by the relationship $f = [(k_{cat}/K_m)_{dATP\ or\ dGTP}/(k_{cat}/K_m)_{dCTP}]$ (*41*). Insertion of dATP opposite Gh/Ia and Sp (duplex **1/5**) yielded similar K_m and k_{cat} values (Table 1). For insertion of dGTP opposite Gh/Ia, the K_m value was 5.5 times lower than the K_m for dGTP insertion opposite Sp (2.9 ± 0.9 vs 16 ± 1.9 μM, respectively). After 15 min of incubation time, insertion of dCTP opposite Gh/Ia and Sp could not be detected for comparison with dATP and dGTP insertion; thus no f values were calculated for the oxidized OG lesions.

UV Melting Experiments. Impact of the Oxidized Lesions on Duplex Stability. In an attempt to determine if there is a correlation between duplex stability and lesion bypass, we studied an assemblage of DNA duplexes designed to mimic the template/primer systems used herein. We studied two sets of 18-mer DNA templates that contained either a high G-C content (XGG18 = 5′-CC**X**GG-3′) or a high A-T content (XAA18 = 5′-TT**X**AA-3′) flanking the lesion site, where **X** was either G, OG, Sp, or Gh/Ia (see Figure 1b). The following group of primers were annealed to these templates: two 13-mer primers (CC13 = 3′-CC... and TT13 = 3′-TT...) annealed immediately upstream of the lesion site and were used as controls; a subset of 14-mer primers (CC14N = 3′-**N**CC... and TT14N = 3′-**N**TT..., where N = A, C, G, T) containing each one of the four canonical bases directly across from the lesion site were analyzed to determine the base-pairing properties of the lesions. Furthermore, the effect of these lesions within a duplex was inspected using an array of 16-mer primers (CC16N = 3′-GG**N**CC... and TT16N = 3′-AA**N**TT..., where N = A, C, G, T) that added two more bases located downstream of the lesion site.

For the XGG18/CC14N and XAA18/TT14N controls, X = G (Tables 2 and 3), the T_ms of the mismatched duplexes (G·A, G·G, G·T) were about the same, and the T_m of the correct G·C was only ∼2−4 or ∼0.4−1.3 °C higher, respectively. As two more G·C base pairs were added to the primer strand (CC16N), the difference between G·C and the mismatches became more pronounced (∼6−11 °C); however, similar addition of two A·T base pairs did not have as large an effect (Tables 2 and 3).

Table 2: Melting Temperatures of Model DNA Duplexes Used To Mimic Template/Primer Systems Where the Template Contains G, OG, Gh/Ia, or Sp Placed in the Following Sequence Context: 5′-CC-X-GG-3′ (Figure 1b)

template	XGG18	X = G (°C)	T_m (°C)	ΔG^{37} (kcal/mol)	X = 8-oxoG (°C)	T_m (°C)	ΔG^{37} (kcal/mol)	X = Gh/Ia (°C)	T_m (°C)	ΔG^{37} (kcal/mol)	X = Sp (°C)	T_m (°C)	ΔG^{37} (kcal/mol)
primers													
13-mer	CC13	52.4 ± 0.4		−11.2 ± 0.3	52.8 ± 0.5		−11.2 ± 0.1	52.4 ± 0.2		−11.0 ± 0.2	52.3 ± 0.70		−10.6 ± 0.2
14-mers	CC14A	54.6 ± 0.8	2.2	−11.5 ± 0.2	55.3 ± 0.7	2.4	−11.4 ± 0.7	55.2 ± 2.1	2.8	−11.5 ± 0.3	52.8 ± 0.5	0.5	−10.5 ± 0.2
	CC14C	57.4 ± 0.8	5.0	−12.0 ± 0.6	56.4 ± 0.6	3.6	−12.5 ± 0.6	55.6 ± 2.9	3.2	−11.5 ± 0.4	52.4 ± 1.7	0.1	−10.2 ± 0.5
	CC14G	55.3 ± 0.8	2.9	−11.9 ± 0.4	55.2 ± 0.2	2.4	−12.0 ± 0.2	54.0 ± 0.5	1.6	−11.5 ± 0.2	54.0 ± 0.6	1.7	−10.6 ± 0.4
	CC14T	53.7 ± 0.7	1.3	−11.3 ± 0.4	53.7 ± 0.6	0.9	−11.8 ± 0.4	50.5 ± 2.3	−1.9	−10.7 ± 0.1	52.8 ± 0.8	0.5	−10.4 ± 0.3
16-mers	CC16A	58.0 ± 0.8	5.6	−13.8 ± 0.7	61.1 ± 0.3	8.3	−14.3 ± 0.4	59.4 ± 0.8	7.0	−11.6 ± 0.1	54.0 ± 1.0	1.7	−10.3 ± 0.2
	CC16C	65.2 ± 0.3	12.8	−16.6 ± 1.1	64.0 ± 0.7	11.2	−15.6 ± 0.6	57.0 ± 1.6	4.6	−11.3 ± 0.2	52.3 ± 1.9	0	−9.9 ± 0.3
	CC16G	58.3 ± 0.7	5.9	−13.9 ± 0.5	57.3 ± 0.6	4.5	−12.5 ± 0.6	54.6 ± 0.6	2.2	−11.3 ± 0.3	54.8 ± 0.8	2.5	−11.2 ± 0.2
	CC16T	57.8 ± 0.3	5.4	−13.9 ± 0.3	56.7 ± 0.4	3.9	−12.7 ± 0.3	50.1 ± 0.6	−2.3	−10.2 ± 0.3	51.3 ± 1.0	−1.0	−10.4 ± 0.2

Table 3: Melting Temperatures of Model DNA Duplexes Used To Mimic Template/Primer Systems Where the Template Contains G, OG, Gh/Ia, or Sp Placed in the Following Sequence Context: 5′-TT-X-AA-3′ (Figure 1b)

template	XAA18	X = G (°C)	T_m (°C)	ΔG^{37} (kcal/mol)	X = 8-oxoG (°C)	T_m (°C)	ΔG^{37} (kcal/mol)	X = Gh/Ia (°C)	T_m (°C)	ΔG^{37} (kcal/mol)	X = Sp (°C)	T_m (°C)	ΔG^{37} (kcal/mol)
primers													
13-mer	TT13	47.1 ± 0.5		−9.8 ± 0.1	47.6 ± 0.7		−10.0 ± 0.1	45.7 ± 0.3		−9.2 ± 0.2	46.1 ± 0.8		−9.4 ± 0.2
14-mers	TT14A	47.5 ± 0.4	0.4	−10.0 ± 0.1	47.7 ± 0.5	0.1	−10.1 ± 0.2	48.9 ± 2.6	3.2	−10.0 ± 0.3	48.8 ± 1.8	2.7	−9.4 ± 0.3
	TT14C	51.3 ± 0.3	4.2	−11.4 ± 0.2	50.5 ± 0.5	2.9	−10.9 ± 0.3	48.2 ± 1.8	2.5	−9.7 ± 0.2	49.3 ± 1.6	3.2	−9.7 ± 0.3
	TT14G	48.3 ± 0.3	1.2	−10.2 ± 0.1	49.2 ± 0.7	1.6	−10.4 ± 0.1	47.6 ± 0.6	1.9	−9.9 ± 0.2	47.7 ± 1.3	1.6	−9.8 ± 0.3
	TT14T	48.3 ± 0.5	1.2	−10.1 ± 0.1	48.4 ± 0.6	0.8	−10.0 ± ±0.1	47.5 ± 2.1	1.8	−9.3 ± 0.2	45.3 ± 0.6	−0.8	−9.3 ± 0.2
16-mers	TT16A	46.1 ± 0.5	−1.0	−9.6 ± 0.1	49.1 ± 0.5	1.5	−10.8 ± 0.2	48.7 ± 0.7	3.0	−9.3 ± 0.1	44.5 ± 1.2	−1.6	−8.8 ± 0.2
	TT16C	54.8 ± 0.4	7.7	−12.8 ± 0.3	53.3 ± 0.2	5.7	−11.9 ± 0.3	47.0 ± 2.3	1.3	−9.1 ± 0.4	47.2 ± 1.6	1.1	−9.2 ± 0.2
	TT16G	47.4 ± 0.5	0.3	−9.6 ± 0.2	46.9 ± 0.5	−0.7	−9.7 ± 0.1	45.5 ± 1.1	−0.2	−9.4 ± 0.3	47.0 ± 1.9	0.9	−9.3 ± 0.2
	TT16T	46.5 ± 0.6	−0.6	−9.9 ± 0.1	46.1 ± 0.8	−1.5	−9.5 ± 0.2	43.8 ± 2.3	−1.9	−8.9 ± 0.3	43.2 ± 0.5	−2.9	−8.7 ± 0.1

OG-containing duplexes (XGG18/CC14N and XAA18/TT14N, X = OG) yielded similar T_m values for G·A, G·G, and G·T mismatches. The similarity of T_ms for the OG·C duplexes compared to the G·C duplexes (∼1 °C) suggests that both G and OG pair most favorably with cytosine. For the GC-rich template (Table 2), addition of two more bases significantly stabilized the OG·C and OG·A duplexes by 4.4 and 3.1 kcal/mol compared to the 13-mer control (ΔT_m = 11.2 and 8.2 °C, respectively). Upon examination of the AT-rich series, the sequence context around the lesion became apparent, because with the addition of two As (XAA18/TT16N, X = OG), the OG·C and OG·A duplexes were not stabilized to the same extent compared to the GC-rich series. Surprisingly, the OG·G, and OG·T mismatches were greatly destabilized relative to the 13-mer control.

When Gh/Ia lesions were introduced into the GC-rich template (Table 2), all duplexes had approximately the same T_m values, except Gh/Ia·T which destabilized the duplex by 1.9 °C. In the 16-mer group (XGG18/CC16N, X = Gh/Ia) the most stable interaction was seen with Gh/Ia·A, suggesting that Gh/Ia interacts most favorably with A ($\Delta\Delta G$ = 0.6 kcal/mol). Since a negative ΔT_m was observed for Gh/Ia·T in both GC- and AT-rich duplexes, this pairing interaction is likely the least favorable. The presence of Sp within the template was especially detrimental to the duplex stability regardless of the opposite interacting base. Once again, the GC-rich duplexes were more stable than their AT-rich counterparts.

DISCUSSION

In the present study we examined the effect of two new guanosine oxidation products on the activity of a model DNA polymerase, the *E. coli* Klenow fragment of polymerase I. Our laboratory recently found that OG could be quantitatively oxidized with ∼95% selectivity in an oligomer by the commercially available one-electron oxidant Na_2IrCl_6 (*38*). Mass spectrometry data obtained from short DNA oligonucleotides confirmed that OG oxidation at 4 and 65 °C leads to the formation of two products with different masses, M − 10 and M + 16, respectively. Template **1** (X = OG) was

oxidized with Na_2IrCl_6 at temperatures ranging from 4 to 65 °C (Figure 2), and the products were identified by ESI-MS in comparison to detailed characterization of the same products in nucleosides (*28*, *29*). In agreement with previously obtained results (*28*, *39*),the products of OG oxidation in the context of 40-mer template **1** were identified as Gh/Ia (M − 10) and Sp (M + 16) from low- vs high-temperature oxidation, respectively. In nucleosides, the M − 10 product was thought to be an equilibrating mixture of Gh and Ia (*29*). Since the composition of the mixture is presently unknown in the context of an oligomer, and indeed may also depend on the presence and identity of the base opposite, the mixture is collectively referred to as Gh/Ia.

Single nucleotide insertion and primer extension have been studied using DNA polymerase Klenow fragment Kf exo$^+$ and Kf exo$^-$. The 40-mer template **1** with an OG base at position X (Figure 1a) was used as a control, and comparisons were also made to an abasic site and to an unmodified G (template **1**, X = Ab, G). While the expected insertion of dCMP and dAMP was observed in the case of unoxidized OG, dAMP and dGMP were inserted opposite the oxidized forms of OG. Under the conditions employed, both Gh/Ia (Figure 3a, low-temperature results) and Sp (high-temperature results) show approximately the same pattern of insertion of dAMP and dGMP with a preference of about 2:1. The insertion of dAMP and dGMP at noncoding lesions, such as abasic sites, has been previously reported in vitro (*23*, *46*, *47*). Also, a recent mechanistic study concerning γ-irradiated OG lesions proposed an abasic site as the main product of OG damage (*48*). To test whether dAMP and dGMP insertion opposite an oxidized OG in our system was in part due to an abasic site formation, a template 40-mer, **1**, with X = Ab, was designed (Figure 1a). The comparison with an abasic site showed the same preference but much lower rates for X = Ab (Figure 3b). Moreover, DNA synthesis in the presence of all four dNTPs was completely inhibited by an abasic site, whereas with oxidized OG lesions a detectable amount of fully extended primer was always present. These results do not support formation of an abasic site as the main product of OG damage as proposed by Doddridge et al. (*48*). In addition, previously reported mass spectrometric studies (*38*, *39*) of the oxidized OG-containing oligomer and ESI-MS analysis of the oxidized template **1** have not presented any evidence for Ab site formation. Standing start primer extension analysis in the presence of all four dNTPs demonstrated that Gh/Ia and Sp lesions represent a strong block for primer extension across the lesion sites. However, traces of fully extended primer were also observed.

We also performed primer extension experiments with oxidized template **1**/primer **5** using Klenow fragment containing the 3′→5′ exonuclease domain (Kf exo$^+$) for proofreading. As anticipated, the amounts of both single nucleotide and full extension were diminished due to the proofreading, and in particular, degradation of the primer became noticeable in studies with Gh/Ia and Sp in the template (Figure 4). While detectable amounts of dAMP and the correct dCMP are inserted opposite unmodified OG in the template by Kf exo$^+$, only traces of dAMP and dGMP are observed opposite oxidized lesions in the template. Thus, Gh/Ia and Sp are better substrates for editing by Kf exo$^+$ than unoxidized OG.

The DNA sequence surrounding a lesion can heavily influence the outcome of base insertion opposite the lesion and subsequent elongation from the resulting lesion terminus. Models for nonslipped and slipped translesion synthesis (TLS) pathways were proposed that can give rise to error-free TLS or base substitution mutation opposite the lesion site and frame-shift mutations, respectively (*2*, *4*, *25*, *49*−*55*).

To analyze the effect of running start DNA synthesis in different sequence contexts, templates **2** and **3** were hybridized with primers **6**, **7**, and **8**. In the design of these template/primer systems we attempted to keep the GC vs AT content approximately the same at the 3′ end of the primer in order to minimize the effects of the duplex stability in that region of DNA while varying the two bases immediately 3′ to the OG site. Studies by Efrati et al. with human DNA polymerase β demonstrated that OG in the template possesses mutagenic potential by "acting at a distance" and can stimulate nucleotide misincorporation at adjacent upstream and downstream template sites (*56*). In our system, neither OG nor oxidized lesions induced misinsertion at the adjacent 3′ sites, and Kf exo$^-$ inserted the correct dTMPs opposite two As and dCMPs opposite two Gs in templates **2** and **3**, respectively. All of the running start experiments showed higher levels of incorporation of nucleotides opposite the lesions, although the qualitative preference for dAMP and dGMP remained the same for oxidized lesions, and dAMP and dCMP were inserted opposite unoxidized OG. Interestingly, when there is a 5′-...GGGTC(**OG**)GG...-3′ motif as in template **3** (Figure 1a), Kf exo$^-$ extends past the unoxidized OG lesion and apparently inserts the correct dGMP opposite C immediately downstream of OG (Figure 5, lane 19). Even though dATP was not present in the reaction mixture, polymerization continued and the band corresponding to the 27-mer extended primer was observed. This band might be due to the insertion of the correct dCMPs opposite the GGG sequence after polymerase presumably "slips" the primer past T inducing a one-base deletion. Frame-shift mutations occurring in a very sequence-specific manner, especially in repetitive guanine sequences or mutational hot spots of the type $(G)_n$ and $(GpC)_n$, were previously reported for bulky acetylaminofluorene-modified guanine residues (*51*). The mechanism of possible primer misalignment induced by the oxidized lesions in oxidized OG system is currently under investigation in our laboratory.

Significantly, running start experiments using oxidized and unoxidized OG-containing templates showed enhanced full extension when all four dNTPs were present. The data shown in Figure 6 indicate that there is a sequence preference for efficiency of extension when Gh/Ia and Sp are present in the templates and full extension appears to be more efficient for the templates containing two Gs immediately 3′ to the lesions. This suggests that a more stable duplex region (GG/CC) compared to AA/TT provides a better template for extension. This sequence dependence is significant because oxidation of either G (*57*) or OG (*58*) in a sequence context in which G follows on the 3′ side is particularly favorable, suggesting that 5′-XG-3′ and 5′-XGG-3′ oxidized OG lesions will be the most common.

UV melting experiments were used to evaluate the impact of the sequence surrounding the lesion and the overall duplex stability. Tables 2 and 3 list the relevant T_m and ΔG^{37} data obtained from the melting curves. Previous studies on the effect of OG on duplex stability were usually performed on

complementary DNA strands of equal length in which the mismatched base pairs were located in the middle of the duplex (*19*, *59*). We attempted to estimate the correlation between the duplex stability and lesion bypass by Kf exo$^-$ in vitro using a set of duplexes that mimicked the template/primer systems used in the primer extension experiments. Studies of the 13-mer duplexes containing OG in a C(OG)C sequence context (*59*) demonstrated that the OG lesion is stabilizing when A is the opposing residue due to the syn structural accommodation of the lesion in the OG·A duplex (*20*, *60*). Our template/primer systems produced similar results. The stabilizing effect of the OG·A base pairs was more pronounced in the set of 16-mer primers (XGG/CC16A and XAA/TT16A, X = OG; Figure 1b). In the GC-rich sequence (Table 2), the OG·A containing duplex was stabilized by 0.5 kcal/mol compared to the unmodified duplex containing G·A mismatch (Table 2). Interestingly, a somewhat higher degree of stabilization was observed in the AT-rich sequence (1.21 kcal/mol; Table 3).

Analysis of the G·A- and Gh/Ia·A-containing duplexes revealed that the putative Gh/Ia·A base pair thermally stabilized the duplex in both GC- and AT-rich sequences (~1.4 and 2.6 °C, respectively). However, Gh/Ia·A-containing duplexes are destabilized by ~2.2 and 0.3 kcal/mol, respectively, compared to G·A mismatch, suggesting that changes in thermal stability do not necessarily correlate with differences in thermodynamic stability, as previously reported by Plum et al. for OG-containing 13-mer duplexes. Overall, when there was a high AT content flanking the lesion site, Gh/Ia showed some thermodynamic preference for A > C, G, whereas Sp-containing duplexes were stabilized to some extent when paired with G. The Sp·C duplex (SpGG18/CC16C) was destabilized by 0.7 kcal/mol compared to the corresponding 13-mer control (Table 2). When there was a high AT content flanking the lesion site, Gh/Ia was stabilized when paired with A > G, C (14-mer series, Table 3), whereas Sp showed some preference for G in the SpGG18/TT16G duplex. In general, the presence of the Sp lesion had a severe effect on the duplex stability regardless of the opposing base, the primer length, and sequence context.

Analysis of the template/primer systems containing terminal mismatched pairs (XGG/CC14, X = G) demonstrated that the difference in ΔGs between correct G·C vs G·A, G·G, or G·T mismatches was not as prominent as when these base pairs are stabilized by the two additional GC pairs on the 5′ side (Table 2). However, when G·A and G·G mismatched duplexes are further extended by two AT base pairs (XAA/TT16N, X = G), the duplexes were destabilized compared to the 13-mer control and corresponding 14-mer systems (Table 3). Furthermore, pairing with T seems to have a destabilizing effect in both GC and AT sequence contexts. This destabilizing effect is particularly apparent in Gh/Ia·T and Sp·T duplexes (Tables 2 and 3), and this correlates with the fact that insertion of T was never observed opposite these lesions in primer extension studies.

Upon the transition from 14-mer primers (duplexes mismatched at the 3′ terminus) to 16-mer primers containing two additional base pairs beyond the mismatched site, Gh/Ia·C and Sp·C duplexes demonstrated decreases in either thermal (ΔT_m) or thermodynamic ($\Delta\Delta G$) stability. The conclusion might be drawn that distortions in the duplex induced by the lesions make base pairing with the "correct" C unfavorable and further extension of these base pairs unlikely. This is also in agreement with single nucleotide insertion and primer extension studies.

To more carefully examine the behavior of lesions with Kf exo$^-$, steady-state kinetics experiments were carried out using template **1** and primer **5**. The results of these studies are summarized in Table 1 and represent the averages of experiments performed at least three times. The results demonstrate that k_{cat} suffers by 50−70-fold for Gh/Ia and Sp lesions compared to the insertion of dCMP opposite unmodified G in the template. The difference in k_{cat} is less dramatic when compared with insertion of dCMP, dAMP, and dGMP opposite OG and corresponds to less than an order of magnitude. K_m increases by 100−170-fold for oxidized OG lesions compared to the correct dCMP insertion opposite G. K_m values for the OG·A pair are 50 times lower than the corresponding values for Gh/Ia·A and Sp·A. However, K_m values for Gh/Ia·G and Sp·G are slightly lower than that for the OG·G pair (2.9 ± 0.9 and 16 ± 1.9 μM vs 48 ± 12 μM). Interestingly, Sp·A, Gh/Ia·A, and Sp·G "mismatches" yielded similar k_{cat}/K_m ratios, while the k_{cat}/K_m for the Gh/Ia·G pair is about an order of magnitude higher. This might be due to the slightly better hydrogen-bonding opportunities that the Gh and Ia isomers provide when paired with G. In addition, either Gh or Ia could exist in enol tautomers yielding a planar hydantoin heterocycle that could be intrahelical and well stacked. Insertion of dCMP was never observed opposite the oxidized lesions, suggesting again that the oxidative event that produced Gh/Ia and Sp causes significant distortions in the duplex or does not provide appropriate hydrogen-bonding opportunities for cytosine, and dCTP is no longer a substrate for the polymerase in this case.

In conclusion, our results provide evidence that chemical lesions produced from one-electron oxidation of OG induce misinsertion of dAMP and dGMP during in vitro DNA synthesis and cause a significant block for DNA elongation. However, our findings for in vitro running start DNA synthesis raise the possibility that the lesions can be more easily bypassed by polymerases in an appropriate sequence context. These data suggest that it will be important to understand the effect of the lesions on duplex structure in different sequences and to investigate base-pairing features between the lesions and the purines A and G by means of NMR studies. In addition, studies of the effect of the terminal oxidized lesions on the efficiency of primer elongation and the insertion of oxidized dOGTP lesions opposite normal bases using different DNA polymerases are also of interest in order to wholly estimate the in vitro mutagenic potential of Gh/Ia and Sp lesions. These studies are currently in progress in our laboratory. Studies of the base excision repair activity of various DNA glycosylases such as Fpg, yOgg1, yOgg2, and hOgg1 toward guanidinohydantoin and spiroiminodihydantoin are also under way (*38*, *61*).

ACKNOWLEDGMENT

We thank Profs. Bradley Preston, Sheila David, and Darrell Davis for helpful discussions and Dr. Elliot Rachlin for assistance with mass spectrometric studies.

SUPPORTING INFORMATION AVAILABLE

HPLC data for purity of lesion-containing synthetic oligodeoxynucleotides and graphical and tabular steady-state

kinetic data for purified diastereomers of Sp and for Gh/Ia. This material is available free of charge via the Internet at http://pubs.acs.org.

REFERENCES

1. Fujikawa, K., Kamiya, H., and Kasai, H. (1998) *Nucleic Acids Res. 26*, 4582−4587.
2. Baynton, K., and Fuchs, R. P. P. (2000) *Trends Biochem. Sci. 25*, 74−79.
3. Bebenek, K., and Kunkel, T. A. (2002) *Cell Mol. Life Sci. 59*, 54−57.
4. Eckert, K. A., and Opresko, P. L. (1999) *Mutat. Res. 424*, 221−236.
5. Tretyakova, N. Y., Niles, J. C., Burney, S., Wishnok, J. S., and Tannenbaum, S. R. (1999) *Chem. Res. Toxicol. 12*, 459−466.
6. Halliwell, B., and Gutteridge, J. M. C. (1999) *Free Radicals in Biology and Medicine*, Claredon Press, Oxford.
7. Ames, B. N., Shigenaga, M. K., and Hagen, T. M. (1993) *Proc. Natl. Acad. Sci. U.S.A. 90*, 7915−7922.
8. Wang, D., Kreutzer, D. A., and Essigmann, J. M. (1998) *Mutat. Res. 400*, 99−115.
9. Cadet, J., Bellon, S., Berger, M., Bourdat, A.-G., Douki, T., Duarte, V., Frelon, S., Gasparutto, D., Muller, E., Ravanat, J.-L., and Sauvaigo, S. (2002) *Biol. Chem. 383*, 933−943.
10. Shigenaga, M. K., Aboujaoude, E. N., Chen, Q., and Ames, B. N. (1994) *Methods Enzymol. 234*, 16−33.
11. Shibutani, S., Takeshita, M., and Grollman, A. P. (1991) *Nature 349*, 431−434.
12. Lowe, L. G., and Guengerich, F. P. (1996) *Biochemistry 35*, 9840−9849.
13. Michaels, M. L., Tchou, J., Grollman, A. P., and Miller, J. H. (1992) *Biochemistry 31*, 10964−10968.
14. David, S. S., and Williams, S. D. (1998) *Chem. Rev. 98*, 1221−1261.
15. Michaels, M. L., Cruz, C., Grollman, A. P., and Miller, J. H. (1992) *Proc. Natl. Acad. Sci. U.S.A. 89*, 7022−7025.
16. Nash, H. M., Bruner, S. D., Shaerer, O. D., Kawate, T., Addona, T. A., Spooner, E., Lane, W. S., and Verdine, G. L. (1996) *Curr. Biol. 6*, 1230−1233.
17. Bruner, S. D., Nash, H. M., Lane, W. S., and Verdine, G. L. (1998) *Curr. Biol. 8*, 393−403.
18. Lu, R., Nash, H. M., and Verdine, G. L. (1997) *Curr. Biol. 7*, 397−407.
19. Barone, F., Cellai, L., Giordano, C., Matzeu, M., Mazzei, F., and Pedone, F. (2000) *Eur. Biophys. J. 28*, 621−628.
20. McAuley-Hecht, K. E., Leonard, G. A., Gibson, N. J., Thompson, J. B., Watson, W. P., Hunter, W. N., and Brown, T. (1994) *Biochemistry 33*, 10266−10270.
21. Oda, Y., Uesugi, S., Ikehara, M., Nishimura, S., Kawase, Y., Ishikawa, Y., Inoue, H., and Ohtsuka, E. (1991) *Anal. Biochem. 197*, 389−395.
22. Venkatarangan, L., Sivaprasad, A., Johnson, F., and Basu, A. (2001) *Nucleic Acids Res. 29*, 1458−1463.
23. Goodman, M. F., Cai, H., Bloom, L. B., and Eritja, R. (1994) *Ann. N.Y. Acad. Sci. 726*, 132−143.
24. Shibutani, S., Fernandes, A., Suzuki, N., Zhou, L., Johnson, F., and Grollman, A. P. (1999) *J. Biol. Chem. 274*, 27433−27438.
25. Kunkel, T. A., and Bebenek, K. (2000) *Annu. Rev. Biochem. 69*, 497−529.
26. Steenken, S., Jovanovic, S. V., Bietti, M., and Bernhard, K. (2000) *J. Am. Chem. Soc. 122*, 2373−2374.
27. Niles, J. C., Burney, S., Singh, S. P., Wishnok, J. S., and Tannenbaum, S. R. (1999) *Proc. Natl. Acad. Sci. U.S.A. 96*, 11729−11734.
28. Luo, W., Muller, J. G., Rachlin, E. M., and Burrows, C. J. (2000) *Org. Lett. 2*, 613−616.
29. Luo, W., Muller, J. G., Rachlin, E. M., and Burrows, C. J. (2001) *Chem. Res. Toxicol. 14*, 927−938.
30. Niles, J. C., Wishnok, J. S., and Tannenbaum, S. R. (2001) *Org. Lett. 3*, 963−966.
31. Adam, W., Arnold, M. A., Grune, M., Nau, W. M., Pischel, U., and Saha-Möller, C. R. (2002) *Org. Lett. 4*, 537−540.
32. Adam, W., Arnold, M. A., Nau, W. M., Pischel, U., and Saha-Möller, C. R. (2002) *J. Am. Chem. Soc. 124*, 3893−3904.
33. Suzuki, T., Masuda, M., Friesen, M. D., and Ohshima, H. (2001) *Chem. Res. Toxicol. 14*, 1163−1169.
34. Suzuki, T., and Ohshima, H. (2002) *FEBS Lett. 516*, 67−70.
35. Sugden, K. D., Campo, C. K., and Martin, B. D. (2001) *Chem. Res. Toxicol. 14*, 1315−1322.
36. Cadet, J., Ravanat, J.-L., Buchko, G. W., Yeo, H. C., and Ames, B. N. (1994) *Methods Enzymol. 274*, 79−89.
37. Adam, W., Saha-Möller, C. R., and Schönberger, A. (1996) *J. Am. Chem. Soc. 118*, 9233−9238.
38. Leipold, M. D., Muller, J. G., Burrows, C. J., and David, S. S. (2000) *Biochemistry 39*, 14984−14992.
39. Duarte, V., Muller, J. G., and Burrows, C. J. (1999) *Nucleic Acids Res. 27*, 496−502.
40. Shibutani, S., Takeshita, M., and Grollman, A. P. (1997) *J. Biol. Chem. 272*, 13916−13922.
41. Goodman, M. F., Creighton, S., Bloom, L. B., and Petruska, J. (1993) *Crit. Rev. Biochem. Mol. Biol. 28*, 83−126.
42. Morales, J. C., and Kool, E. T. (2000) *Biochemistry 39*, 2626−2632.
43. Breslauer, K. J. (1994) *Methods Mol. Biol. 26*, 347−372.
44. Muller, J. G., Duarte, V., Hickerson, R. P., and Burrows, C. J. (1998) *Nucleic Acids Res. 26*, 2247−2249.
45. Goyal, R. N., Jain, N., and Garg, D. K. (1997) *Bioelectrochem. Bioenerg. 43*, 105−114.
46. Gentil, A., Renault, G., Madzak, C., Margot, A., Cabral-Neto, J. B., Vasseur, J. J., Imbach, J. L., and Sarasin, A. (1990) *Biochem. Biophys. Res. Commun. 173*, 704−710.
47. Clark, J. M. (1988) *Nucleic Acids Res. 16*, 9677−9685.
48. Doddridge, Z. A., Cullis, P. M., Jones, G. D. D., and Malone, M. E. (1998) *J. Am. Chem. Soc. 120*, 10998−10999.
49. Shibutani, S., and Grollman, A. P. (1993) *J. Biol. Chem. 268*, 11703−11710.
50. Minnick, D. T., Astatke, M., Joyce, C. M., and Kunkel, T. A. (1996) *J. Biol. Chem. 271*, 24959−24961.
51. Hoffman, G., and Fuchs, R. P. P. (1997) *Chem. Res. Toxicol. 10*, 347−359.
52. Bloom, L. B., Chen, X., Fygenson, D. K., Turner, J., O'Donnell, M., and Goodman, M. F. (1997) *J. Biol. Chem. 272*, 27919−27930.
53. Lingbeck, J. M., and Taylor, J.-S. (1999) *Biochemistry 38*, 13717−13724.
54. Osheroff, W. P., Beard, W. A., Yin, S., Wilson, S. H., and Kunkel, T. A. (2000) *J. Biol. Chem. 275*, 28033−28038.
55. Iyer, R. R., Pluciennik, A., Rosche, W. A., Sinden, R. R., and Wells, R. D. (2000) *J. Biol. Chem. 275*, 2174−2184.
56. Efrati, E., Tocco, G., Eritja, R., Wilson, S. H., and Goodman, M. F. (1999) *J. Biol. Chem. 274*, 15920−15926.
57. Saito, I., Nakamura, T., Nakatani, K., Yoshioka, Y., Yamaguchi, K., and Sugiyama, H. (1998) *J. Am. Chem. Soc. 120*, 12686−12687.
58. Hickerson, R. P., Prat, F., Muller, J. G., Foote, C. S., and Burrows, C. J. (1999) *J. Am. Chem. Soc. 121*, 9423−9428.
59. Plum, G. E., Grollman, A. P., Johnson, F., and Breslauer, K. J. (1995) *Biochemistry 34*, 16148−16160.
60. Kouchakdjian, M., Bodepudi, V., Shibutani, S., Eisenberg, M., Johnson, F., Grollman, A. P., and Patel, D. J. (1991) *Biochemistry 30*, 1403−1420.
61. Hazra, T. K., Muller, J. G., Manuel, R. C., Burrows, C. J., Lloyd, R. S., and Mitra, S. (2001) *Nucleic Acids Res. 29*, 1967−1974.

BI0264925